Shape matters: Near-field fluid mechanics dominate the collective motions of ellipsoidal squirmers

K. Kyoya,[1] D. Matsunaga,[1] Y. Imai,[1] T. Omori,[1] and T. Ishikawa[1,2,*]
[1]*Department of Bioengineering and Robotics, Tohoku University, Sendai 980-8579, Japan*
[2]*Department of Biomedical Engineering, Tohoku University, Sendai 980-8579, Japan*
(Received 7 May 2015; published 28 December 2015)

Microswimmers show a variety of collective motions. Despite extensive study, questions remain regarding the role of near-field fluid mechanics in collective motion. In this paper, we describe precisely the Stokes flow around hydrodynamically interacting ellipsoidal squirmers in a monolayer suspension. The results showed that various collective motions, such as ordering, aggregation, and whirls, are dominated by the swimming mode and the aspect ratio. The collective motions are mainly induced by near-field fluid mechanics, despite Stokes flow propagation over a long range. These results emphasize the importance of particle shape in collective motion.

DOI: 10.1103/PhysRevE.92.063027 PACS number(s): 47.63.mf, 47.54.−r, 47.57.E−, 47.63.Gd

I. INTRODUCTION

Microswimmers exhibit a wide variety of collective behaviors. For instance, swimming bacteria generate mesoscale coherent structures in dense suspensions [1–3] and orientational order in confined suspensions [4,5]. Swimming magnetotactic bacteria form bands in a magnetic field [6]. Spermatozoa form trains [7] and vortex arrays in the vicinity of a wall [8]. Due to its biological importance, the mechanism of collective motions has been investigated extensively in fluid mechanics [9–13].

Several studies have investigated the coherent structures in bacterial suspensions using continuum models, in which cells were assumed to be sufficiently small compared with the flow field of interest [3,11–20]. By considering the alignment of cells in the stretching direction of background flow, the continuum models successfully reproduced the turbulent-like spatiotemporal motions of bacteria. These results illustrate that the coherent structures can be reproduced by considering only far-field fluid mechanics effects and that near-field cell-cell interactions may not be as important.

By contrast, discrete models have been used to calculate the collective motions of individual cells [20–26]. When two cells come into close proximity, some of the earlier discrete models introduced an *ad hoc* force to direct two nearby cells in parallel, although the physical meaning of the interaction force was vague. Some studies dealt precisely with near-field fluid mechanics, but the number of cells was limited to two [27–30]. Several other studies were able to provide a precise solution of the hydrodynamic interactions among multiple cells; however, the cell shape was restricted to a spherical form [31–36]. Despite these extensive research efforts, the effect of cell shape and near-field fluid mechanics on the collective motion of microswimmers remains unclear.

Recently Kantsler *et al.* [37] reported the importance of near-contact interactions on the surface scattering of swimming microorganisms, even in the Stokes flow regime. We consider that the near-contact interactions between cells should also play an important role in the scattering angle between cells and ultimately the collective motions. Sokolov and Aronson [38] experimentally demonstrated the importance of collisional interactions in the collective motions of *Bacillus subtilis*. Because the collisional interactions are strongly dependent on the detailed configuration of the cells, the cell shape should play an important role in the collective motions.

In this paper we investigate the effect of near-field fluid mechanics on the collective motions of microswimmers. We precisely solve the Stokes flow of interacting swimmers, including the lubrication flow between two nearby surfaces, in a monolayer suspension. The results showed that various collective motions, such as ordering, aggregation, and whirls, are dominated by the swimming mode and aspect ratio. The collective motions are mainly induced by the near-field fluid mechanics, despite Stokes flow propagation over a long range. These results emphasize the importance of particle shape in collective motion.

II. BASIC EQUATIONS AND NUMERICAL METHODS

The microswimmer considered has a spherical or ellipsoidal form and propels itself by generating surface tangential velocities, i.e., a squirmer [39,40]. The squirmer model has been used to analyze collective motions in previous studies [31–36]. The surface tangential velocity u_s of an ellipsoidal squirmer is given by [41]

$$u_s = \alpha \sqrt{\frac{2}{[1+(b/a)^2]-[1-(b/a)^2]\cos(2\theta)}} \times (\sin\theta + \beta \sin\theta\cos\theta), \quad (1)$$

where a and b are the major and minor axes of the ellipsoidal squirmer, respectively. The aspect ratio c is given by $c = a/b$; α defines the swimming velocity of a solitary squirmer V_0 in an unbounded fluid; θ is the angle from the orientation vector of the squirmer; β controls the second mode of the squirming velocity. A squirmer with positive β is a puller, analogous to having thrust-generating apparatus at the front of the body. A squirmer with a negative β is a pusher.

The governing equation of the Stokes flow field external to the squirmers is given by [42]

$$\boldsymbol{u}(\boldsymbol{x}_0) = \sum_i \int_{S_i} \boldsymbol{q}(\boldsymbol{x}) \cdot \boldsymbol{T}(\boldsymbol{x},\boldsymbol{x}_0) \cdot \boldsymbol{n}(\boldsymbol{x}) dS_i(\boldsymbol{x}) + \boldsymbol{v}(\boldsymbol{x}_0), \quad (2)$$

where $\boldsymbol{q}$ is the double-layer potential, $\boldsymbol{n}$ is the normal vector, $\boldsymbol{v}$ is the velocity due to short-range repulsive forces between

*ishikawa@pfsl.mech.tohoku.ac.jp

squirmers, and S_i is the surface of the squirmer i. $\boldsymbol{T}$ is Green's function given by

$$\boldsymbol{T}(\boldsymbol{x},\boldsymbol{x}_0) = \epsilon_{ijk}\frac{r_k}{r^3}, \tag{3}$$

where $\boldsymbol{\epsilon}$ is the unit alternating isotropic tensor, $\boldsymbol{r} = \boldsymbol{x} - \boldsymbol{x}_0$ and $r = |\boldsymbol{r}|$. The velocity boundary condition on the surface of squirmer i is given by

$$\boldsymbol{u}(\boldsymbol{x}_0) = \boldsymbol{V}_i + \boldsymbol{\Omega}_i \wedge (\boldsymbol{x}_0 - \boldsymbol{x}_{c,i}) + \boldsymbol{u}_s(\boldsymbol{x}_0), \quad \boldsymbol{x}_0 \in S_i, \tag{4}$$

where $\boldsymbol{x}_{c,i}$ is the center of squirmer i. The distribution of $\boldsymbol{q}$ was calculated by inserting Eq. (4) into Eq. (2). $\boldsymbol{V}_i$ and $\boldsymbol{\Omega}_i$ are the translational and rotational velocities of squirmer i, given by [43]

$$\boldsymbol{V}_i = -\frac{4\pi}{S_i}\int_{S_i} \boldsymbol{q}(\boldsymbol{x})\, dS_i(\boldsymbol{x}), \tag{5}$$

$$\boldsymbol{\Omega}_i = -\frac{3}{2}\left(\frac{4\pi}{S_i}\right)^2 \int_{S_i} (\boldsymbol{x}_0 - \boldsymbol{x}_{c,i}) \wedge \boldsymbol{q}(\boldsymbol{x})\, dS_i(\boldsymbol{x}). \tag{6}$$

We assumed a monolayer suspension, such that the centers and orientation vectors of all squirmers remained in the same plane, although the flow field was fully three-dimensional (3D). This treatment allowed us to observe collective motion at a larger scale than in a 3D suspension. The computational cost of a standard boundary element method is enormous and increases the cube of the particle number when we use a single layer potential. The computational cost can be reduced to the square of the particle number when a double layer potential is used, as in Eq. (2). To further reduce the computation time, Eq. (2) was expanded into multipoles, and the numerical code was implemented for general purpose computation on graphics processing units (GPGPUs), as explained in Ref. [44]. Our code could achieve a computational speed of 590 GFLOPS (Giga Floating point number Operations Per Second) for double precision calculations, which is approximately one order of magnitude faster than the theoretical performance of the latest CPU. Moreover, by exploiting the planar symmetry of the monolayer suspension, we could reduce the number of computational meshes to around half. Even with these technical efforts, the maximum number of particles we could compute to observe long-time collective motions with a high precision in the near-field fluid mechanics was limited to approximately 100. Thus, we decided to investigate a monolayer suspension in this study; a 3D suspension will be investigated in future work.

One hundred squirmers were initially placed in random positions and orientations in a unit square domain; their subsequent motion was then calculated. The infinite extent of the monolayer was given by the periodic boundary conditions. Hydrodynamic interactions between mirror squirmers in periodic domains were calculated up to three layers; the rate of strain induced by additional layers was negligibly small. The surface of each squirmer was then discretized into 1280 triangular elements. The time integral was performed by the second-order Runge-Kutta scheme. A short-range repulsive force was added to the system to avoid the problem of overlapping particles under finite time step conditions, as in our previous study [32]. The effect of the repulsive force on the trajectories of the cells was small. It acts only in the very near-field and changes the distance between particles by only 10^{-3}. The reason why the repulsive force plays such a minor role in the suspension of squirmers may be explained as follows. The translational and rotational velocities generated by two nearby squirmers were analyzed by Ishikawa *et al.* [27]. The leading order term of the relative velocities between two squirmers in the lubrication theory is the surface squirming velocity, $\boldsymbol{u}_s$, of $O(1)$. This term does not appear in a system with inert particles, which is the essential difference between a suspension of inert particles and squirmers. The next leading order term of the relative velocities is $F/[\log(\lambda^{-1}) + O(1)]$, where F is the force and λ is the minimum separation between two squirmers. The second leading order term $\log(\lambda^{-1})$ is a very weak singularity and thus dominates the solution only in a mathematical sense. Thus, the relative velocities between squirmers are dominated in the main by $\boldsymbol{u}_s$, and the repulsive force does not significantly affect the trajectories of the cells. The areal fraction of squirmers at the center plane ϕ_a was set at 0.3, except in Fig. 3. The swimming mode β and aspect ratio c were varied over the ranges $-3 \leqslant \beta \leqslant 3$ and $1 \leqslant c \leqslant 3$, respectively.

III. RESULTS AND DISCUSSION

The collective motion of pullers ($\beta = 1$), neutral swimmers ($\beta = 0$), and pushers ($\beta = -1$), with spherical $c = 1$ and ellipsoidal ($c = 3$) cell shapes, are shown in Fig. 1. The yellow arrows in the figure indicate velocity vectors, and the gray lines show the orientations. Supplemental movies of these six cases are also provided online [42]. The puller swimmers tended to aggregate [Fig. 1(a) and 1(d)]. Supplemental Movie 1 shows that the aggregation appeared to be stronger in the ellipsoidal case than in the spherical case. In the case of neutral swimmers with a spherical shape [Fig. 1(b)], the motion tended to be in the same direction, i.e., ordered motion, with a certain distance between particles. Neutral swimmers with an ellipsoidal shape [Fig. 1(e)] also showed ordering, but the distance between swimmers was narrower than in the spherical case. Figure 1(c) shows spherical pushers; in this case, no obvious pattern was recognized. By contrast, for the case of ellipsoidal pushers [Fig. 1(f)], a few neighboring squirmers tended to swim in similar directions. These results indicate qualitatively that the collective motions are strongly affected by the swimming mode and aspect ratio.

In Fig. 1 we show the results with $\beta = 1$, 0, and -1 to emphasize the difference in the collective behaviors. Although the collective motions of pushers with $\beta = -1$ was weak, strong collective motions was observed for pushers with $\beta = -0.3$. The results are provided as Supplemental Movie 4 [42]. To discuss the correlations between the present study and former experimental studies using bacteria, here we derive the effective beta value of bacteria such as *Escherichia coli* . According to Ishikawa *et al.* [27], β is the ratio of second mode squirming to the first mode, i.e., B_2/B_1. Because the stresslet St is correlated to B_2 by $St = 4\pi\mu a^2 B_2$, and the swimming velocity U is correlated to B_1 by $U = 2B_1/3$, β can be expressed as $\beta = St/(6\pi\mu a^2 U)$. The stresslet St has the dimension of force multiplied by length. Therefore, we can estimate St by multiplying the strength of the drag and thrust forces and the length between the two forces. By

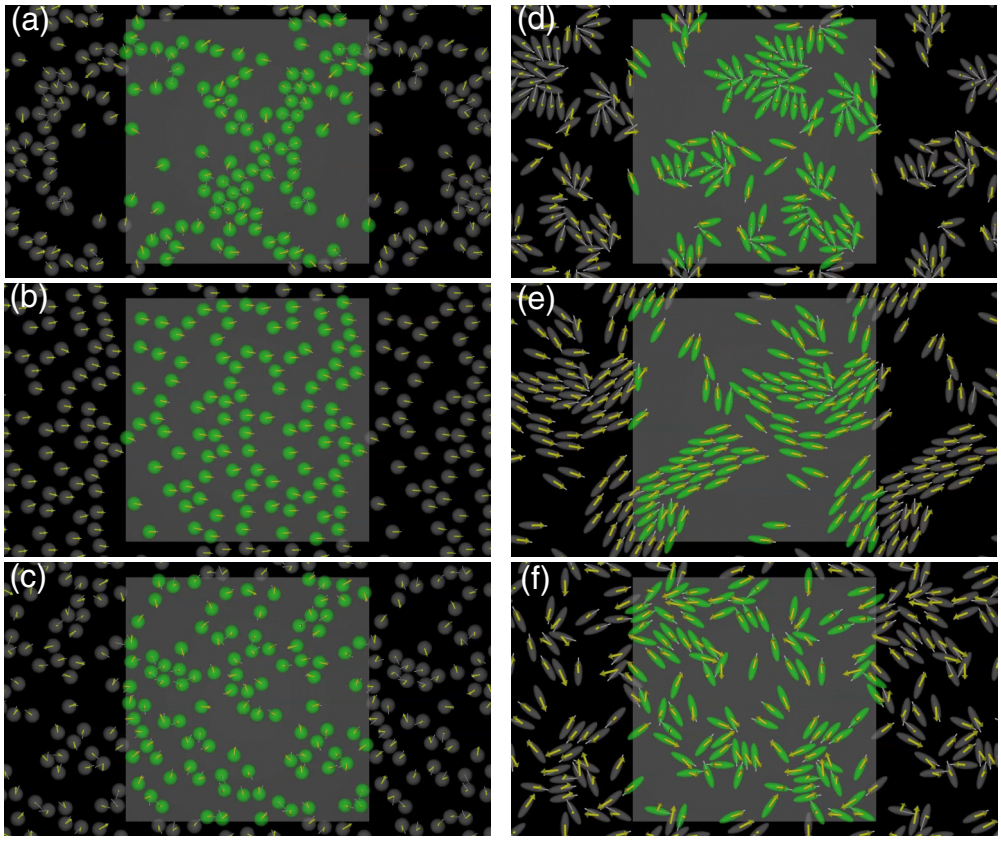

FIG. 1. (Color online) Sample snapshots of squirmers in a monolayer suspension. The yellow arrows indicate velocity vectors, and the gray lines indicate the orientation ($\phi_a = 0.3$): (a), (d) pullers ($\beta = 1$), (b), (e) neutral swimmers ($\beta = 0$), and (c), (f) pushers ($\beta = -1$). The aspect ratio c has a value of 1 for (a)–(c) and 3 for (d)–(f). Supplemental movies of these six cases are provided online [42].

assuming that a sphere of radius a expresses a whole cell consisting of a cell body with diameter $0.5a$ and flagella with length $1.5a$, the magnitude of the drag and thrust forces can be estimated as $1.5\pi\mu aU$ and the distance between the two forces as a. By inserting $St = -1.5\pi\mu a^2 U$, we finally obtain $\beta = -1.5\pi\mu a^2 U/(6\pi\mu a^2 U) = -0.25$. This discussion illustrates that the β of actual bacteria, such as *E. coli*, can be estimated to be smaller than unity. Because we observed strong collective motions with $\beta = -0.3$, as shown in Supplemental Movie 4 [42], the present results do not conflict with former experimental observations.

We first analyze the ordering of neutral swimmers. The strength of ordering can be described by the polar order parameter E, defined as $E = |\langle \boldsymbol{e} \rangle|$, where $\boldsymbol{e}$ is the orientation vector of a squirmer, and $\langle\rangle$ represents the suspension average. The change in E over time for spherical ($c = 1$) and ellipsoidal ($c = 3$) squirmers, under various initial conditions, is shown in Fig. 2(a). For spherical squirmers, E is close to one, without strong fluctuations, when $tV_0/a \geqslant 100$. This indicates that all squirmers eventually orient to the same direction, and that the direction does not fluctuate considerably. By contrast, for ellipsoidal squirmers, the E curve fluctuates considerably, and the mean value is about 0.8. Therefore, ellipsoidal squirmers do not order as strongly as their spherical counterparts, and the orientations fluctuate in space and time. This result may seem counterintuitive, because the orientation change can be restricted more strongly by the surrounding squirmers as the aspect ratio is increased, i.e., the excluded volume effect. The alignment of elongated particles can already be attributed to volume exclusion together with the persistence of motion because it exerts a torque. When a high-aspect-ratio squirmer that leads a flock is struck from the side by another squirmer, however, it changes its orientation more easily than a spherical squirmer, due to its slenderness. As such, the squirmers that follow also change their orientation according to the leading squirmer, due to the small amount of space between the surrounding squirmers. This may be why ellipsoidal squirmers

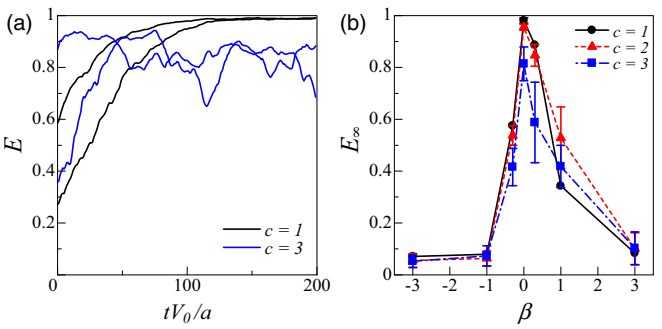

FIG. 2. (Color online) Effect of aspect ratio c on the ordering of squirmers ($\phi_a = 0.3$): (a) time change of the polar order parameter E ($\beta = 0$) and (b) long-time polar order parameter E_∞ under various β conditions.

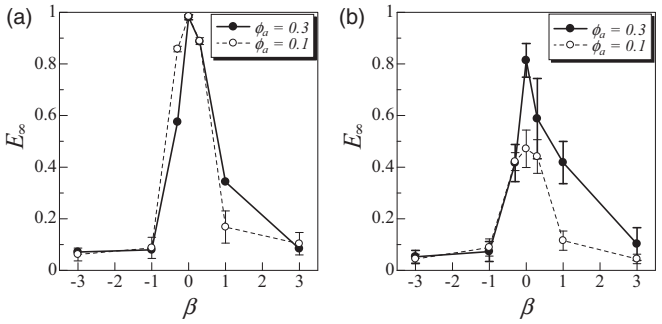

FIG. 3. Effect of areal fraction ϕ_a on the long-time polar order parameter E_∞ under various β conditions: (a) aspect ratio $c = 1$ and (b) $c = 3$.

experience larger spatiotemporal fluctuations, compared with spherical squirmers. We note that we also performed some trial simulations including the rotational diffusivity of squirmers. The results showed that the polar order did not disappear when the rotational diffusivity was sufficiently small.

Figure 2(b) shows the long-time polar order parameter, E_∞, with various c and β conditions. E_∞ is averaged for $tV_0/a \geqslant 100$ with different initial conditions; the error bars indicate the standard deviation. We see that E_∞ reached its maximum value when $\beta = 0$, i.e., for neutral swimmers, and decreased as $|\beta|$ increased. The fluctuations in E_∞, indicated by the standard deviation, are large in the case of ellipsoidal swimmers. These results illustrate that the ordering structure is affected considerably by the swimming mode β and the cell shape c.

We then investigated the effect of the areal fraction ϕ_a on the long-time polar order parameter, as shown in Fig. 3. In the case of $c = 1$, the ordering of cells appears in a similar manner even with $\phi_a = 0.1$. In the case of $c = 3$, on the other hand, the ordering of cells was reduced as ϕ_a decreased; however, the ordering phenomenon did not disappear even with $\phi_a = 0.1$. These results illustrate that the collective motions observed in the present study were not qualitatively affected by ϕ_a, when ϕ_a was in the range $\phi_a = 0.1$–0.3.

Next, we analyze the aggregation of pullers and the whirl structures of pushers. Figure 4(a) shows the average swimming velocity of squirmers $\langle V \rangle$, normalized by V_0, under various c and β conditions. We see that $\langle V \rangle / V_0$ becomes greater than 1 when $c = 3$ and $\beta = -3$. Such an increase in the swimming velocity was also reported in former experimental studies using bacteria [1,2], although the increase in the former experiments was larger than in the present study. The quantitative difference may arise from the difference in the aspect ratio between the present study and bacteria used in the former studies. The aspect ratio of *E. coli*, including the flagella bundle, is approximately 8–10, and that of *Bacillus subtilis* is approximately 10, which is considerably larger than the present study of $c = 3$. In the case of pullers with $c = 3$, on the other hand, a significant decrease was observed in $\langle V \rangle$. This is because elongated pullers tend to aggregate into clusters (cf. Supplemental Movie 1 [42]). Squirmers become effectively stuck in the cluster formation, and their swimming velocities decrease considerably. The large decrease in $\langle V \rangle$ was observed only for ellipsoidal squirmers, which again illustrates the importance of particle shape on collective motion.

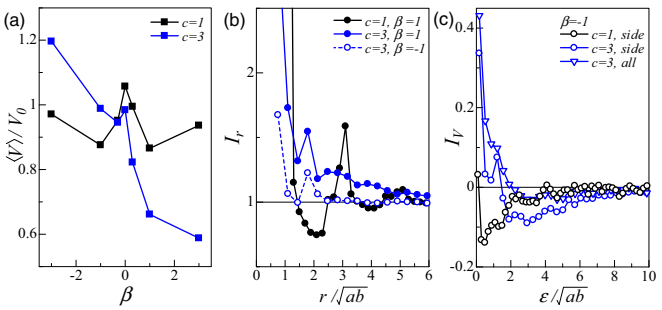

FIG. 4. (Color online) Effect of c and β on the flow structures ($\phi_a = 0.3$): (a) average swimming speed of squirmers; (b) radial distribution function, where r is the surface-to-center distance; and (c) velocity correlation, where ε is the surface-to-surface distance.

Figure 4(b) shows the radial distribution function I_r defined by $I_r(r) = \langle \lambda(r) \rangle / \lambda_0$, where λ_0 is the average number density of particles in the monolayer and $\lambda(r)$ is the number density of particles at a distance of r away from the surface of a given reference particle. We use the distance r between the surface and center, instead of two centers, because it provides larger peaks in the I_r curves of ellipsoidal squirmers. We see that I_r of $\beta = 1$, $c = 1$ has clear peaks at $r = 1$ and 3, which indicates a crystal structure. The case of I_r of $\beta = 1$, $c = 3$ also indicates particle aggregation, although that of $\beta = -1$ does not. The peaks of $\beta = 1$, $c = 3$ are not as clear as those of $c = 1$, because the distance varies with the relative orientation of two nearby ellipsoids.

Figure 4(c) shows the velocity correlation, I_V, among pushers ($\beta = -1$). Here *side* indicates that the correlation is calculated only when a squirmer is present lateral to the reference squirmer, i.e., $\pm\pi/4$ from the orthogonal direction, whereas *all* indicates that the correlation is calculated for all particles. Here we use the surface-to-surface distance ε along the horizontal axis to emphasize the positive correlation among nearby squirmers. For the case $c = 3$, I_V is positive in the small ε region, but negative in the large ε region, which defines the whirl structure. The negative correlation is stronger for *side* than *all*. For spherical squirmers, however, the whirl structure can be clearly discerned in the figure.

These results clearly indicate that the aspect ratio of squirmers significantly affects the collective motion. However, it is still unclear whether the difference in collective motion was caused by near-contact interactions or interactions via the long-propagating Stokes flow. Therefore, trial simulations were performed that neglected the far-field fluid mechanics. Here the velocity field equation presented in Eq. (2) is modified as follows:

$$\boldsymbol{u}(\boldsymbol{x}_0) = \sum_{\text{inear}} \int_{S_{\text{inear}}} \boldsymbol{q}(\boldsymbol{x}) \cdot \boldsymbol{T}(\boldsymbol{x}, \boldsymbol{x}_0) \cdot \boldsymbol{n}(\boldsymbol{x})\, dS_{\text{inear}}(\boldsymbol{x}) + \boldsymbol{v}(\boldsymbol{x}_0). \tag{7}$$

Here *inear* is the number of squirmers in the near field. The threshold distance for the near-field is set as $\varepsilon < 3\sqrt{ab}$. The cutoff length should be sufficiently short to delete far-field interactions. However, too short a cutoff length may neglect even the near-field fluid mechanics. To minimize far-field fluid

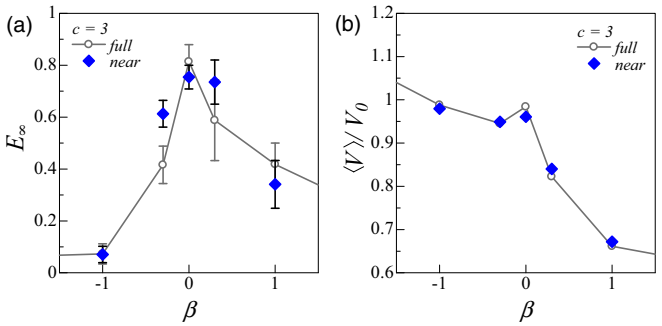

FIG. 5. (Color online) Comparisons between the results of a full simulation and those with only near-field interactions ($c = 3$ and $\phi_a = 0.3$): (a) long-time polar order parameter E_∞ and (b) average swimming speed of squirmers.

mechanics while maintaining the near-field fluid mechanics, we set the cutoff length as $3\sqrt{ab}$. We note that the results were not sensitive to ε when $2\sqrt{ab} \leqslant \varepsilon \leqslant 4\sqrt{ab}$. Equation (7) completely neglects the traction forces generated on the surface of the squirmers at $\varepsilon \geqslant 3\sqrt{ab}$, and far-field squirmers cannot generate background stretching flow. Figure 5 compares the long-time polar order parameter E_∞ and average swimming speed $\langle V \rangle$ for full and near-field simulations using Eq. (6). The near-field simulations captured basic tendencies, such as ordering and aggregation, well. Consequently, the collective motions examined in this study were generated mainly by near-field fluid mechanics.

By considering the importance of the near-field fluid mechanics, we may be able to understand the mechanism of collective motions from nearest-neighbor two-body interactions. The angle between two orientation vectors of nearest-neighbor squirmers $\theta_{\rm near}$ is defined such that $\theta_{\rm near} > 0$ when two squirmers are approaching, but $\theta_{\rm near} < 0$ when they swim away from each other, as shown in the inset of Fig. 6(a). We calculated the time derivative $d\theta_{\rm near}/dt$, i.e., the relative rotational velocity; the results of $\langle d\theta_{\rm near}/dt \rangle$ are shown in Fig. 6(a) ($c = 3$). We see that the relative rotational velocity of nearest-neighbor squirmers changes dramatically with β.

We further analyzed the nearest-neighbor two-body interactions in the simulations with many squirmers. The bar graphs in Figs. 6(b)–6(d) show the probability density of nearest-neighbors P as a function of $\theta_{\rm near}$, whereas the line graphs show $d\theta_{\rm near}/dt$ ($c = 3$). When $\beta = 1$ [Fig. 6(b)], two squirmers collide near $0 < \theta_{\rm near} < 90^\circ$ and do not rotate afterwards. These squirmers tend to stay close for a long time, as shown schematically in the inset, which causes the aggregation shown in Fig. 1(d). We note that the schematic shows only two nearby squirmers; other surrounding cells are omitted for simplicity. When $\beta = 0$ (Fig. 6(c)), the colliding squirmers tend to orient parallel to each other and retain this orientation for some time, as shown schematically in the inset. This tendency is consistent with the ordering structure shown in Fig. 1(e). When $\beta = -1$

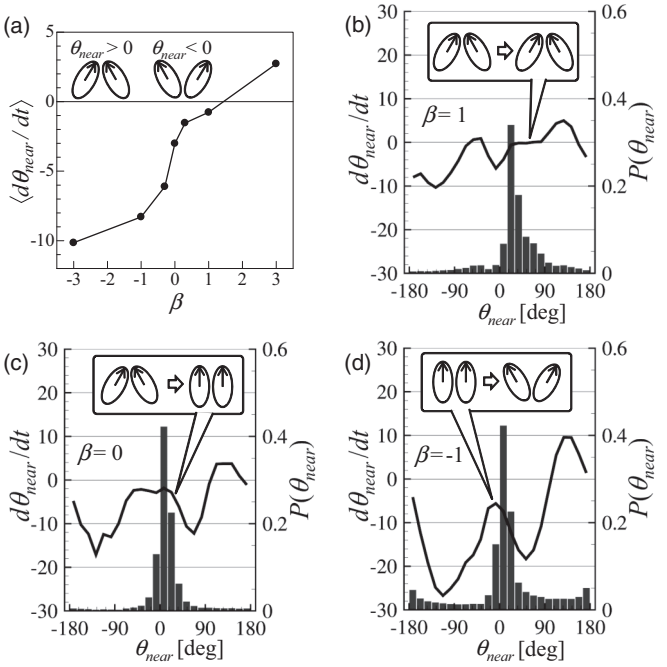

FIG. 6. Interactions between two nearby squirmers. Angle of the orientation vector relative to that of the nearest neighbor, $\theta_{\rm near}$, is expressed in degrees ($c = 3$ and $\phi_a = 0.3$): (a) effect of β on $d\theta_{\rm near}/dt$; and (b)–(d) bar graphs show the probability density P and line graphs $d\theta_{\rm near}/dt$. The insets show the orientation change of two nearby squirmers schematically.

[Fig. 6(d)], the squirmers, having collided, first orient parallel to each other. They cannot retain parallel orientation for a long time and swim away from each other, as shown in the inset. This tendency is again consistent with the collective motion observed in Fig. 1(f). These results illustrate that the mechanism of collective motion can be understood in terms of nearest-neighbor two-body interactions.

IV. CONCLUSION

In summary, we showed that various collective motions, such as ordering, aggregation, and whirls, can be reproduced by considering hydrodynamic interactions between squirmers. The collective motions are induced mainly by near-field fluid mechanics and are strongly affected by the aspect ratio and swimming mode of squirmers. Nearest-neighbor two-body interactions explain the mechanism of collective motions well. These results reveal the importance of particle shape in collective motion, even in the Stokes flow regime.

ACKNOWLEDGMENT

This work was supported by JSPS KAKENHI (Grants No. 25000008 and No. 26242039).

[1] C. Dombrowski, L. Cisneros, S. Chatkaew, R. E. Goldstein, and J. O. Kessler, Phys. Rev. Lett. **93**, 098103 (2004).

[2] T. Ishikawa, N. Yoshida, H. Ueno, M. Wiedeman, Y. Imai, and T. Yamaguchi, Phys. Rev. Lett. **107**, 028102 (2011).

[3] J. Dunkel, S. Heidenreich, K. Drescher, H. H. Wensink, M. Bär, and R. E. Goldstein, Phys. Rev. Lett. **110**, 228102 (2013).
[4] H. Wioland, F. G. Woodhouse, J. Dunkel, J. O. Kessler, and R. E. Goldstein, Phys. Rev. Lett. **110**, 268102 (2013).
[5] E. Lushi, H. Wioland, and R. E. Goldstein, Proc. Natl. Acad. Sci. USA **111**, 9733 (2014).
[6] D. C. Guell, H. Brenner, R. B. Frankel, and H. Hartman, J. Theor. Biol. **135**, 525 (1988).
[7] H. Moore, K. Dvoráková, N. Jenkins, and W. Breed, Nature (London) **418**, 174 (2002).
[8] I. H. Riedel, K. Kruse, and J. Howard, Science **309**, 300 (2005).
[9] T. Ishikawa, J. R. Soc. Interface **6**, 815 (2009).
[10] T. J. Pedley, Exp. Mech. **50**, 1293 (2010).
[11] S. Ramaswamy, Annu. Rev. Condens. Matter Phys. **1**, 323 (2010).
[12] D. L. Koch and G. Subramanian, Annu. Rev. Fluid Mech. **43**, 637 (2011).
[13] M. C. Marchetti, J. F. Joanny, S. Ramaswamy, T. B. Liverpool, J. Prost, M. Rao, and R. A. Simha, Rev. Mod. Phys. **85**, 1143 (2013).
[14] C. W. Wolgemuth, Biophys. J. **95**, 1564 (2008).
[15] D. Saintillan and M. J. Shelley, Phys. Fluids **20**, 123304 (2008).
[16] A. Baskarana and M. C. Marchettia, Proc. Natl. Acad. Sci. USA **106**, 15567 (2009).
[17] A. Peshkov, I. S. Aranson, E. Bertin, H. Chaté, and F. Ginelli, Phys. Rev. Lett. **109**, 268701 (2012).
[18] T. Brotto, J.-B. Caussin, E. Lauga, and D. Bartolo, Phys. Rev. Lett. **110**, 038101 (2013).
[19] S. P. Thampi, R. Golestanian, and J. M. Yeomans, Phys. Rev. Lett. **111**, 118101 (2013).
[20] H. H. Wensink, J. Dunkel, S. Heidenreich, K. Drescher, R. E. Goldstein, H. Löwena, and J. M. Yeomans, Proc. Natl. Acad. Sci. USA **109**, 14308 (2012).
[21] J. P. Hernandez-Ortiz, C. G. Stoltz, and M. D. Graham, Phys. Rev. Lett. **95**, 204501 (2005).
[22] T. Vicsek and A. Zafeiris, Phys. Rep. **517**, 71 (2012).
[23] D. Saintillan and M. J. Shelley, Phys. Rev. Lett. **99**, 058102 (2007); J. R. Soc. Interface **9**, 571 (2012).
[24] O. Pohl and H. Stark, Phys. Rev. Lett. **112**, 238303 (2014).
[25] I. Llopis and I. Pagonabarraga, Europhys. Lett. **75**, 999 (2006).
[26] H. H. Wensink and H. Lowen, J. Phys.: Condens. Matter **24**, 464130 (2012).
[27] T. Ishikawa, M. P. Simmonds, and T. J. Pedley, J. Fluid Mech. **568**, 119 (2006).
[28] C. M. Pooley, G. P. Alexander, and J. M. Yeomans, Phys. Rev. Lett. **99**, 228103 (2007).
[29] R. M. Navarro and I. Pagonabarraga, Eur. Phys. J. E **33**, 27 (2010).
[30] I. Llopis and I. Pagonabarraga, J. Non-Newtonian Fluid Mech. **165**, 946 (2010).
[31] T. Ishikawa and T. J. Pedley, Phys. Rev. Lett. **100**, 088103 (2008).
[32] T. Ishikawa, J. T. Locsei, and T. J. Pedley, J. Fluid Mech. **615**, 401 (2008).
[33] R. A. Lambert, F. Picano, W.-P. Breugem, and L. Brandt, J. Fluid Mech. **733**, 528 (2013).
[34] A. Zottl and H. Stark, Phys. Rev. Lett. **112**, 118101 (2014).
[35] M. Potomkin, V. Gyrya, I. Aranson, and L. Berlyand, Phys. Rev. E **87**, 053005 (2013).
[36] A. A. Evans, T. Ishikawa, T. Yamaguchi, and E. Lauga, Phys. Fluids **23**, 111702 (2011).
[37] V. Kantsler, J. Dunkel, M. Polin, and R. E. Goldstein, Proc. Natl. Acad. Sci. USA **110**, 1187 (2013).
[38] A. Sokolov and I. S. Aranson, Phys. Rev. Lett. **109**, 248109 (2012).
[39] M. J. Lighthill, Commun. Pure Appl. Math. **5**, 109 (1952).
[40] J. R. Blake, J. Fluid Mech. **46**, 199 (1971).
[41] S. R. Keller and T. Y. Wu, J. Fluid Mech. **80**, 259 (1977).
[42] See Supplemental Material at http://link.aps.org/supplemental/10.1103/PhysRevE.92.063027 for movies of collective motions of squirmers.
[43] C. Pozrikidis, J. Fluid Mech. **568**, 161 (2006).
[44] D. Matsunaga, Y. Imai, T. Omori, T. Ishikawa, and T. Yamaguchi, J. Biomech. Sci. Eng. **9**, 14 (2014).